Applied Surface Science 631 (2023) 157563

Contents lists available at ScienceDirect

Applied Surface Science

journal homepage: www.elsevier.com/locate/apsusc

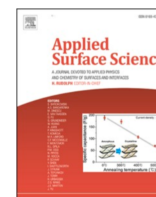

Full Length Article

A comprehensive atomistic picture of the as-deposited Ni-Si interface before thermal silicidation process

César Jara Donoso [a,*], Antoine Jay [a], Julien Lam [b], Jonas Müller [a], Guilhem Larrieu [a], Georges Landa [a], Corrado Bongiorno [c], Antonino La Magna [c], Alessandra Alberti [c], Anne Hémeryck [a,*]

[a] LAAS-CNRS, Université de Toulouse, CNRS, Toulouse, France
[b] CEMES-CNRS, Toulouse, France
[c] CNR IMM, Catania, Italy

A B S T R A C T

Despite numerous technological applications associated to nickel silicide thin films, their formation mechanisms are still far from being understood. We combined experimental and numerical approaches to unravel the early stages of nickel silicide formation with an atomistic precision. In particular, we employed first principles calculations, X-ray reflectivity as well as high-resolution scanning transmission electron microscopy analyses. Altogether, our work demonstrates that during nickel deposition on top of a silicon surface, an interface alloyed layer is formed even at room temperature before any thermal activation. Moreover, we managed to determine that this interfacial layer has a nickel-rich Ni_3Si composition which is favored by the ability of nickel atoms to penetrate the surface layers of the silicon substrate.

1. Introduction

Transition metal silicides have been used since several decades in the microelectronics industry to reduce contact resistances at the active areas of transistors and to ensure electrical continuity between transistors and interconnects. They are widely used in all types of technology such as imaging, flash, photonics and CMOS [1–8]. Silicides in microelectronics are formed as a directly integrated material from a silicon substrate, by a solid-state reaction between a metal and the silicon material, forming an alloy compound. Different silicides have been used depending on the technological node and the dimension of the transistor gate associated with smaller and smaller sizes and more and more complex architectures [3,8–13]. Among them, NiSi is one the most promising silicides for the development of new technologies in advanced devices with complex 3D architecture to form high-conductivity nickel silicide/silicon contacts [14]. The thicknesses of Ni used today are less than 10 nm [12,15,16]. NiSi combines all physical properties required for optimal integration with advanced processes: a low silicon consumption preserving the low dimensions of both the Si substrate and silicide layer with a smooth interface, a low formation temperature compatible with low process temperature, and good electrical properties. However, the compatibility of NiSi with the new constraints to access thinner devices and 3D architectures with low-temperature, short-run processes is critical. A perfect control of the silicide layer formation is sought to achieve the desired composition and structure of the target phase NiSi to preserve the expected outstanding properties [17–21]. In particular, it has been shown how the early stages of the Ni-Si interaction impact on the sequence of phases and on their lattice properties [22–25]. Silicidation is indeed driven by what occurs since the first Ni-Si interaction during the nickel deposition step.

Mastering the growth of NiSi directly integrated from a silicon substrate remains a major challenge. The complete reaction pathways involved in NiSi formation are still debated [16,26–30] thus making the industrial integration of Ni-based silicides difficult. It requires an understanding of each of the steps before and after thermal activation, and the associated phase transformation throughout the entire silicidation process. The modeling of the whole silicide process, including the deposition and annealing steps, has not yet been achieved. Indeed, in cases of nickel silicide formation, during deposition, Ni_xSi_y alloys and their polymorphs form rapidly, changing from one phase to another of the phase diagram at temperatures right below 500 °C. The formation of the silicide sequence can be divided into three stages based on the phase diagram [31,32]: Ni-rich, NiSi and $NiSi_2$ phases. In this range of temperature, it is thus possible to form silicon-rich layers, which are then undesirable because of their lower conductivity of less interest for their integration in the devices.

* Corresponding authors.
E-mail addresses: cesar.jara@laas.fr (C.J. Donoso), anne.hemeryck@laas.fr (A. Hémeryck).

https://doi.org/10.1016/j.apsusc.2023.157563
Received 18 December 2022; Received in revised form 5 May 2023; Accepted 17 May 2023
Available online 22 May 2023
0169-4332/© 2023 The Authors. Published by Elsevier B.V. This is an open access article under the CC BY-NC license (http://creativecommons.org/licenses/by-nc/4.0/).

The objective of this paper is to describe the first steps of the nickel silicidation process before the thermal activation step. We detail the deposition phase schematized in Fig. 1. We therefore focus on the material, as-deposited prior to thermal activation, through a precise atomic scale characterization of the alloyed interface layer formed during the deposition of nickel on a silicon substrate, coupling experimental and theoretical tools. The determination of the as-deposited interfacial layer allows to understand the origin of the sequence leading to the different Ni_xSi_y phases during the silicidation process. It allows for determining the structure of the material right before the thermal activation that leads to the final silicide.

In particular, we detail the formation of an interface layer of Ni_3Si alloyed composition. This finding is important as reports in the literature, based on in-situ investigations of the Ni-Si(1 0 0) interfacial reaction during thin film deposition at 300 K, present contradicting results finding either Ni_2Si [33,34] or Ni_3Si [35] as initial mixing layer composition. Successive ex-situ investigations using Transmission Electron Microscopy (TEM) and X-ray reflectivity (XRR) measurements support the observation of such an amorphous Ni-Si mixing layer but have remained unable to provide a clear identification of the composition as either Ni_2Si or Ni_3Si [36]. In contrast, XRR results obtained for thicker Ni films clearly state the formation of Ni_2Si [37] thereby highlighting the suitability of XRR measurements for the phase analysis of such thin layers with amorphous structure.

In the first part, we describe the theoretical methods and the results of the deposition of Ni atoms on a Si surface describing the adsorption, surface diffusion and insertion of Ni on the Si surface until the formation of an alloyed pattern using first principles calculations. In the second part, these calculations are complemented by X-ray reflectivity (XRR) and High-Resolution Scanning Transmission Electron Microscopy (HR-STEM) studies performed on ten nanometer-thick layers of Nickel deposited by thermal evaporation on pre-treated [0 0 1] silicon substrates.

2. Computational Details

Total energy calculations are performed using the density functional theory (DFT) [38,39] as implemented in Quantum Espresso (QE) [40,41]. The Perdew-Burke-Ernzerhof (PBE) [42] generalized gradient approximation of the exchange and correlation functional is used altogether with Projected Augmented Waves pseudo-potentials (PAW) [43]. A plane wave basis set with an energy cutoff of 50 Ry is used to describe the wave functions. The Brillouin zone is sampled at the Gamma point only. The magnetization of Ni disappears as soon as Ni interacts with Si, which permits not to use a spin polarized calculation.

To find the transition state structures and corresponding barrier energies, the activation-relaxation technique (ART [44]) is used in its ART-DFT version [45–47] where it is coupled with a DFT software, here QE, for the force and energy evaluations. Two kinds of calculations are performed: (i) when only the initial structure is known, an exploration of the potential energy surface to obtain all the saddle points and minima surrounding this initial structure, and (ii) when the initial and final structures are known, a convergence to the saddle point from an interpolation of these two structures. The convergence force threshold used to define the transition state structure is 0.05 eV/Å.

The reconstructed Si(0 0 1) surface [48] is simulated using a $2 \times 2 \times 7.5$ supercell of crystalline silicon that contains fifteen layers of sixteen silicon atoms (Fig. 2). The two bottom layers are kept fixed to simulate a bulk effect. A monolayer of thirty-two hydrogen atoms was used to saturate the dangling bonds of the bottom layer of the slab. A vacuum region of 15 Å is placed above the Si(0 0 1) surface. All the atomic positions are relaxed and the supercell parameters are kept fixed. We use a simulation cell with fixed dimensions to match the simulation of the

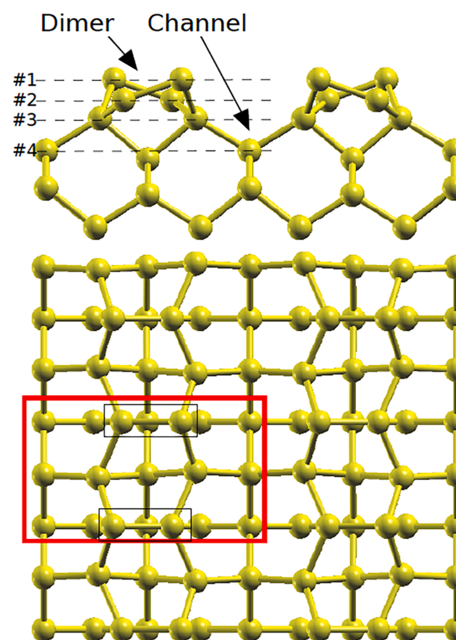

Fig. 2. (top) Side view and (bottom) top view of the Si(0 0 1) surface with dimers rows separated by channels, and the indexed four topmost layers. Red rectangle: region of the surface for the Ni deposition considering the surface symmetries. Black rectangles: positions of the dimers inside the red rectangle. (For interpretation of the references to colour in this figure legend, the reader is referred to the web version of this article.)

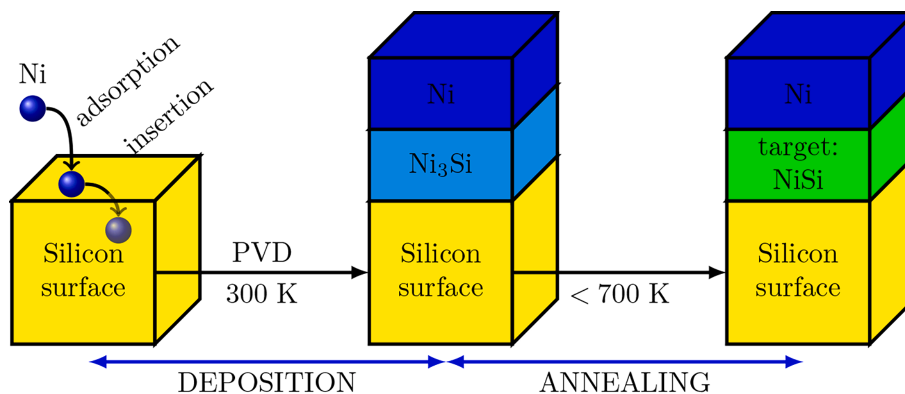

Fig. 1. Schematic representation of the different stages needed to obtain NiSi silicide. The deposition of Ni atoms is first deposited with Physical Vapor Deposition (PVD) at ambient temperature forming an as-deposited interface of Ni3Si composition, which is then annealed at temperature below 700 K to form the targeted NiSi layer.

deposition process considering the fact that the thickness of the silicon is much larger than that of the deposited nickel. We then check that the size of our system in terms of number of layers and atoms per layer is in good correspondence with the conducted study and the simulated coverage so as not to introduce artifacts from the stress in the simulation box.

Adsorption energy E_{ads} of the n-th Ni atom is determined as:

$$E_{ads} = E_{nNi} - E_{(n-1)Ni} - E_{Ni}$$

where E_{nNi} is the energy of the relaxed supercell containing n adsorbed Ni atom(s), $E_{0xNi} = E_{SiSurface}$ is the energy of the Si(001) surface, and E_{Ni} is the energy of an isolated Ni atom.

3. Theoretical results

A step-by-step study using first-principles calculations is described. First, the description of the initial steps of the nickel deposition includes the adsorption of Ni on the reconstructed Si(001) surface, the diffusion of Ni atoms on the surface, and the insertion of Ni atoms into the topmost layers of the silicon substrate. Second, the rapid formation of interface alloy with a nickel-rich Ni_3Si composition is demonstrated, highlighting some thermodynamic effects playing an essential role on the early apparition of the alloyed pattern.

3.1. *Adsorption of Ni atom on Si(001)*

The deposition step starts with the adsorption of Ni atoms on the surface of the silicon substrate. The Ni atom is initially placed on top of several distinct adsorption sites according to the topology of the silicon surface reconstruction [49] on or between two dimers and above the channel. After relaxation, we obtain a catalogue of six stable adsorbed configurations (Appendix A from a to f) described hereafter.

(i) The channel configuration (CH, E_{ads} = -4.58 eV, Fig. 3 and Appendix A.a)) is the most stable configuration reached upon adsorption above the channel. In CH, the Ni atom is adsorbed inside the channel between the third and fourth layers and the Ni atom forms six bonds with the surrounding Si atoms. (ii) When the adsorption occurs between two dimers (DB standing for Dimerbed, E_{ads} = -4.41 eV, Fig. 3 and Appendix A.b)), the Ni atom is located between two adjacent dimers of the same row between the first and second layers. In this configuration, the Ni atom forms six bonds with surrounding Si atoms. (iii) In the middle configuration (MD, E_{ads} = -4.06 eV, Fig. 3 and Appendix A.c)), the Ni atom is located between two silicon atoms of two adjacent dimers of the same row. The Ni atom forms three bonds with the surrounding Si atoms. (iv) In a so-called channel bridge configuration (CB, E_{ads} = -3.85 eV, Fig. 3 and Appendix A.d)), the Ni atom is centered on the channel between the second and third layers and the Ni atom forms three bonds with the surrounding Si atoms. (v) In the so-called dimer row (DR, E_{ads} = -3.71 eV, Appendix A.e)) the Ni atom is situated above a dimer, centered on the row axis and the Ni atom forms two bonds with the surrounding Si atoms. (vi) Finally, in the above channel configuration (AC, E_{ads} = -3.10 eV, Appendix A.f)) the Ni atom is centered on the channel, above the first topmost Si layer and the Ni atom forms two bonds with the surrounding Si atoms.

Looking at the energies of these stable configurations, we have identified the configurations CH and DB as the two most energetically favorable sites of adsorption for the Ni on the Si(001) surface. Noticing that with a small difference of 0.17 eV in the formation energy between them, they are at least 0.35 eV more favorable than the other obtained configurations. This result is consistent with the number of bonds present in these structures. A complementary study is then necessary to definitively confirm that CH and DB sites are the most favorable by studying the surface diffusion, *i.e.* determining the activation barrier, from MD, CB, DR, AC toward CH and DB. In addition, the configurations CH, adsorbed in the channel and DB, adsorbed between two dimers, and in strong interaction with the silicon substrate seem to be good candidates suitable for allowing the insertion of nickel atoms into the topmost layers of the substrate.

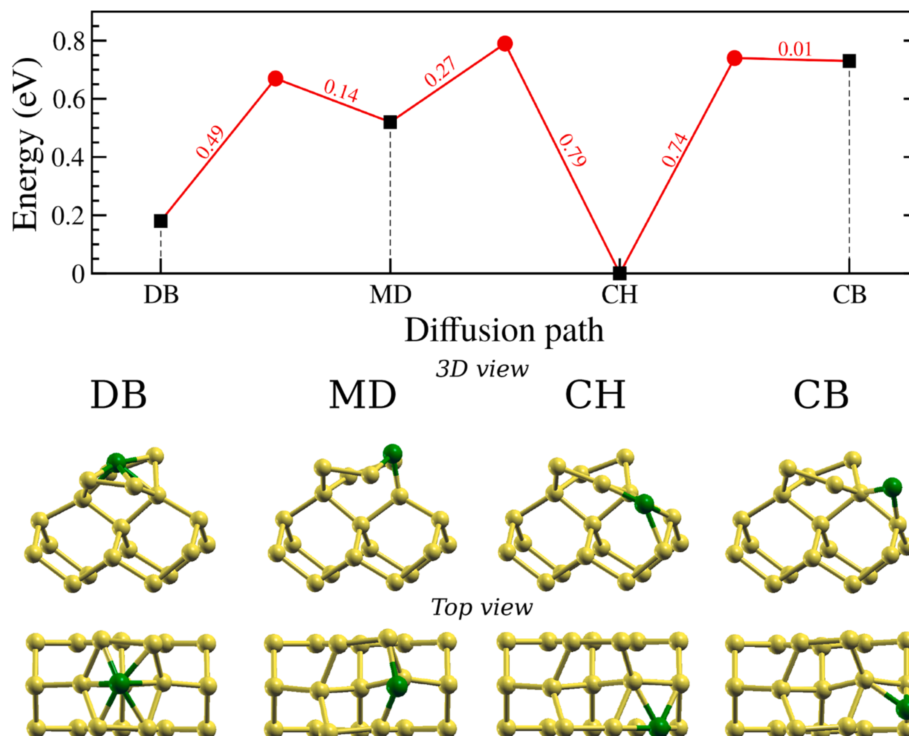

Fig. 3. Energy diagram of the atomic diffusions of one Ni atom adsorbed on the Si(100) surface. Activation barriers (numerical values in red) are given in eV. 3D side and top views of each atomic configuration are provided. (For interpretation of the references to colour in this figure legend, the reader is referred to the web version of this article.)

3.2. Diffusion of Ni atom on Si(001)

The diffusion of Ni atoms on the surface is performed to validate the stability of the most favorable configurations identified in the adsorption study, *i.e.* CH and DB, starting from all the adsorbed stable configurations previously identified. We determine the diffusion paths connecting them to the two most favorable adsorbed configurations, CH and DB schematized on Fig. 3.

The results show small activation barriers ranging from a low value of 0.002 eV to 0.27 eV, altogether with stabilization energies ranging from 0.35 eV to a large value of 0.73 eV. The diffusion from CB to CH requires a small activation barrier of 0.01 eV with a large energy gain of 0.73 eV, suggesting a fast diffusion from CB at the early stages of the deposition process. The diffusion from MD to DB requires an activation barrier of 0.14 eV, with an energy gain of 0.35 eV, in comparison with the diffusion to DC which requires an activation barrier of 0.27 eV, also with a favorable energy gain of 0.52 eV. Note that the diffusion from DR to DB requires a very low activation barrier of 0.002 eV (not plotted).

At this stage, based on the analysis of adsorption and surface diffusion studies, the two most favorable sites of the surface CH and DB are indeed the two most likely configurations on the Si surface at low temperatures due to the low activation barriers and associated energy gains.

3.3. Insertion of Ni specie on Si(001)

The insertion of the nickel atom into the topmost layers of the silicon substrate is studied. The objective is to estimate the ability of Ni to insert into the surface layers of the silicon substrate as a function of the Ni coverage on the surface. This study is carried out first for one Ni atom, and then for two Ni atoms. This insertion step, which follows the adsorption step described above, thus starts from the two most favorable adsorbed configurations CH and DB.

3.3.1. Insertion of Ni specie on Si(001)

The Ni atoms insert successfully from both adsorbed configurations CH and DB finding two new stable inserted configurations. The minimum energy path (MEP) of the insertion from the DB configuration is shown in Fig. 4 from left to right, and the MEP from the CH configuration in Fig. 4 from right to left. The insertion of the Ni atom from the DB configuration is obtained after crossing an activation barrier of 0.32 eV. The system exhibits an energy gain of 1.32 eV compared to the DB configuration. The reached inserted configuration is labeled IDB standing for Inserted Dimer Bed. In this configuration, the Ni atom is located between the third and fourth layers centered below the dimer row and is bonded to six Si atoms present in its vicinity. The insertion from the CH configuration toward an ICH configuration exhibits a low activation barrier of 0.16 eV and is associated to an energy gain of 0.10 eV. The reached configuration is labeled ICH standing for Inserted Channel. In ICH, the Ni atom is located at the fourth layer and is bonded to six Si atoms present in its vicinity. From ICH, a diffusion toward IDB configuration requires a low activation barrier of 0.10 eV, associated with an energy gain of 1.05 eV.

From these two adsorption states DB and CH, the insertion is then favored over diffusion on the surface. The Ni insertion is limited to the topmost layer of the surface below the dimer row, where we have calculated that the diffusion of a nickel atom deeper into the substrate is not favorable and results in less stable configurations than ICH or IDB. The resulting configuration is the first structuring configuration of the alloy formation where the Ni atom is located in IDB configuration.

3.3.2. Insertion of Ni with a second adsorbed Ni atom in the near vicinity

The aim of this section is to study the influence of an already adsorbed Ni atom on the adsorption of a second Ni atom nearby.

This study starts by reading Fig. 5 from left to right, from a configuration where two Ni atoms are adsorbed in two adjacent DB sites on the same dimer row (structure I in Fig. 5). The first insertion of one DB atom has an activation barrier of 0.33 eV and is associated to an energy gain of 1.15 eV compared to the starting DB + DB structure. The reached

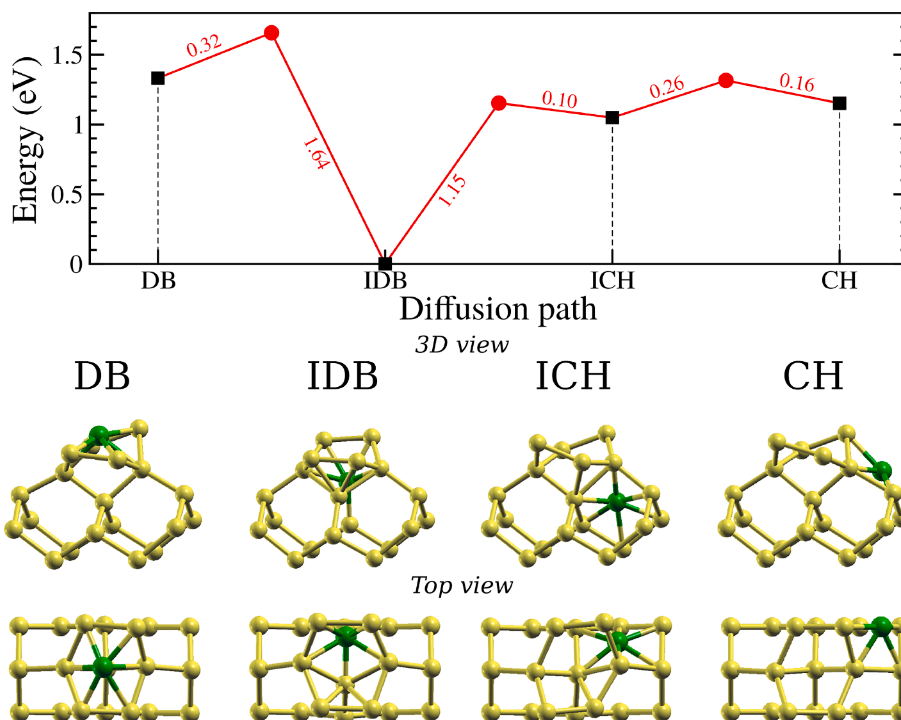

Fig. 4. Insertion paths from DB (from left to right) and CH (from right to left) configurations into the topmost layers of the silicon substrate. The resulting configurations are labeled IDB (InsertedDimerBed) and ICH (InsertedChannel) 3D side and top views of each atomic configuration are provided. Activation barriers (numerical values in red) are given in eV. (For interpretation of the references to colour in this figure legend, the reader is referred to the web version of this article.)

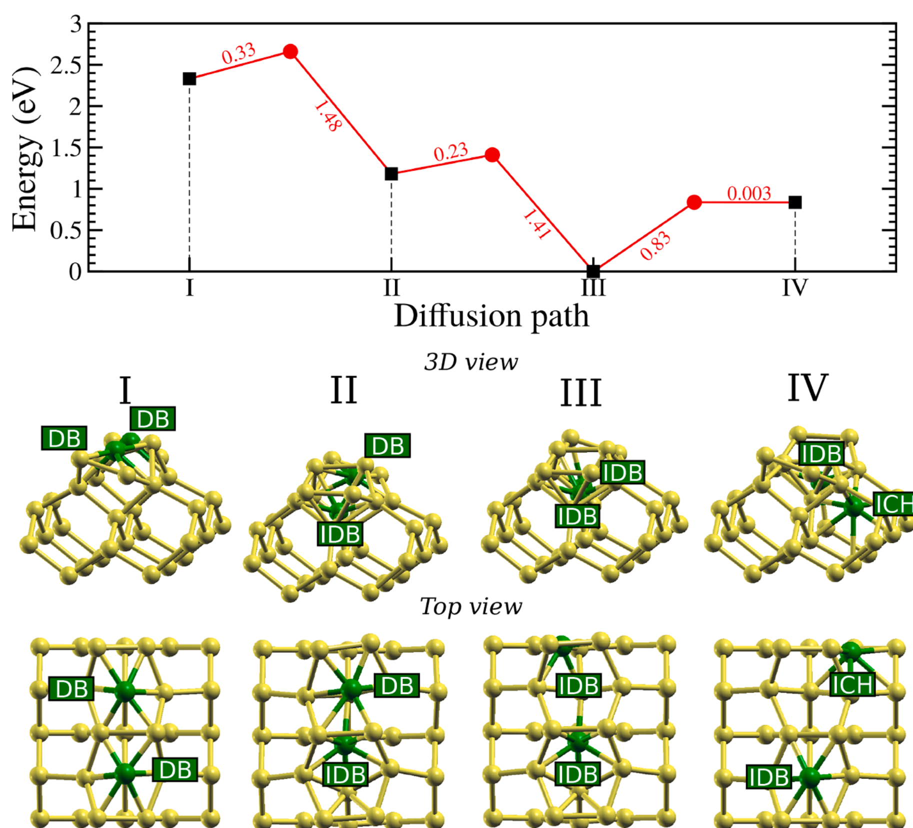

Fig. 5. Most favorable insertion paths of two Ni atoms initially situated in DB configurations (from left to right) and insertion path of two Ni atoms initially situated in IDB + CH configuration (from right to left). Activation barriers (numerical values in red) are given in eV. An additional explored path is given in Appendix B. (For interpretation of the references to colour in this figure legend, the reader is referred to the web version of this article.)

configuration is an IDB + DB configuration (structure II in Fig. 5), where the diffusing Ni atom has reached an IDB configuration. The activation barrier for this insertion of a DB to IDB with another neighboring Ni atom shows that it is not affected by the presence of the neighboring Ni atom (0.33 eV vs 0.32 eV obtained in the case of a single Ni atom, see section 3.3.1). We observe that the energy gain is affected, being 0.17 eV less favorable in comparison with the insertion of one DB atom (section 3.3.1).

From this DB/IDB configuration, the most favorable path is obtained when the DB atom is pushed to also reach an IDB position. This insertion results in two IDBs (structure III in Fig. 5) associated to an energy gain of 1.18 eV, compared to the DB/IDB configuration. This diffusion requires an activation barrier of 0.23 eV: we observe a notable decrease in the activation barrier thanks to the presence of IDB, compared to the insertion of a single DB (0.23 eV vs 0.32 eV discussed in section 3.3.1).

It can be noted that another path has been explored from structure II where the inserted IDB atom is pushed further to reach an ICH position, resulting in a configuration composed of a DB and an ICH. This diffusion requires an activation barrier of 0.86 eV and the system undergoes an energy loss of 0.73 eV, which is an unfavorable diffusion (see Appendix B). From this structure III, the diffusion of one of the IDB atoms toward an ICH position destabilises the system and is therefore not favorable (structure IV in Fig. 5). This finding could suggest that silicidation forms layer by layer, from the top layer to deeper layers, out of the scope of the present paper.

In the following paragraph we describe additional results considering that the starting configurations contain an already inserted IDB configuration. We describe two adsorptions assuming that the second Ni adsorbs near the already inserted IDB.

— the adsorption of a second Ni is performed right above the IDB position (not shown): the added Ni atom relaxes to the DB configuration, and the IDB atom remains unchanged. The adsorption of this second Ni is associated with an adsorption energy of −4.06 eV, *i.e.* 0.35 eV less favorable compared to DB adsorption in the single atom case. We do not observe any local structure change around the IDB site.

— the adsorption of a second Ni is performed above a CH position through the channel in proximity of IDB (depicted in Fig. 5 from right to left). A spontaneous insertion of the Ni atom initially placed on a CH position without activation barrier is observed directly from the channel path towards the ICH configuration reaching a configuration the structure IV (ICH + IDB). We recall that for this insertion from CH to ICH in the case of a single atom, the activation barrier is 0.16 eV. The adsorption of this second Ni is associated with an adsorption energy of −4.85 eV, *i.e.* −0.27 eV more favorable than in the case of the adsorption of a single atom from the gas phase, or more favorable by −0.17 eV when comparing the complete paths to the ICH position. This insertion is favored, because the presence of IDB locally elongates the Si-Si bonds in the channel. In particular, the penetration path modifies the local structure of the adjacent dimer (tilting and bondlength) which offers space to the atom arriving in the channel to insert directly into ICH configuration. The trend described here is consistent with a favorable diffusion process and suggests a rapid formation of an alloyed pattern thanks to the favored insertion of Ni atom without any activation barrier.

In conclusion, we demonstrate that the first stages of the deposition are dominated by Ni diffusion: Ni insertion occurs favorably through the channel of the reconstructed Si(001) surface in the early stages of deposition. This insertion through the channel is strategic for several reasons: — by diffusion with a relatively low activation barrier, Ni diffuses to occupy the sites below the dimer row (more easily than by insertion through the dimer row) — this insertion allows occupation of the sites below the dimer row which then facilitates insertion into the

ICH sites and leads to the stabilization of the system, — diffusion to IDB from ICH lowers the barrier to insert the Ni atom through the dimer row from the DB sites to IDB. We show that the only thermal activation required is due to the presence of dimers on the substrate surface, but that once this first barrier is overcome and the first atoms inserted, the insertion of Ni atoms is favored everywhere on the surface.

3.3.3. Towards the spontaneous formation of an alloyed layer on the surface

The purpose of the following paragraph is to demonstrate that by increasing the Ni coverage on the already identified insertion structures, we can still insert Ni atoms spontaneously, where the Ni and Si atoms self-organize to create an alloyed mixed layer of 3:1 composition. The conducted *ab initio* calculations cannot cover the long-range order effects, but locally validate the 3:1 alloy composition.

Based on the conclusions drawn in the previous section, the starting point is a stable structure initially composed of three Ni atoms in IDB and six Ni atoms in ICH, for a total of nine Ni atoms already inserted in the surface of the silicon substrate. The choice of this structure is justified to avoid any effect related to the size of our simulation box and to avoid periodicity artefacts of the box, while reaching a sufficient number of Ni atoms to observe an alloyed mixing process between Si and Ni. It is checked that the relative pressure in the simulation cell is still acceptable to carry out additional adsorptions. The relaxed configuration is shown in Fig. 6-a-snapshot I, where the green atoms are the Ni atoms. We notice in this final relaxed structure that two of the Ni atoms initially inserted in the ICH position, move out of their ICH position to reach a CH position as described above. We can note here that the displacement of the Ni atoms from ICH to CH contributes to the pure layer alignment of the Ni atoms as can be observed in some Ni_xSi_y alloys.

Using this relaxed structural pattern, we add a Ni atom above the CH position, on a position that we have materialized by a purple atom on the Fig. 6-a, for a total of ten Ni atoms (not all shown for reason of readability of the figure). The final configuration after relaxation of this additional Ni atom is shown in Fig. 6-a-snapshot IV. Upon adsorption of this additional tenth Ni atom, we observe a structural rearrangement, of which is detailed in Fig. 6-b to identify the associated movements of both Si and Ni atoms. We observe that the deposited Ni atom adsorbs on a CH position. During this adsorption, a Ni atom initially located on a ICH site is moved to a new configuration where the Ni atom is inserted deeper in the Si substrate. This site is labelled IB, standing for Inserted Bulk and shown in Fig. 6-a ~~and in panel 4 of~~ Fig. 6-b. At the same time, a Si atom is also moved slightly, to reach a centered position between five Ni atoms. The adsorption energy of this new atom is −4.87 eV. We observe this adsorption energy is more favorable than the CH adsorption on the pure Si surface (-4.87 eV vs −4.58 eV).

Looking more closely at the local pattern formed, we find evidence of an atomic arrangement of Ni and Si atoms as can be observed in Ni_3Si alloys, indicating a favorable interaction between the Ni and Si atoms tending to the formation of a 3:1 compositional mixture. In Fig. 6-c, we present the local pattern extracted from the atomic structure shown in Fig. 6-a. If we compare this pattern with the perfect crystal structures of the Ni_3Si alloy, we clearly identify an organization of the Ni and Si atoms, exhibiting thus the same local chemical environment of Ni as it exists in the Ni_3Si alloy, especially in the (1 1 0) and (0 0 1)-45° orientations, these two patterns being distinguished by the positioning of the Si atoms in the 3rd and 4th layers. We are therefore more interested in describing the atomic pattern formed in particular by looking at the interatomic distances in this local pattern. We compare the interatomic distances, and they present close values with those of the Ni_3Si alloys (2.62 Å and 2.48 Å, and 3.76 Å and 3.51 Å) that is to say weak relative differences of the order of 5.6 % and 7.1 % showing that the interatomic distances of the obtained pattern are close to the distances between the atoms in the Ni_3Si alloy crystal. Analyzing the a/b ratio in Fig. 6-c we observe a value of 0.69. A similar value of 0.70 is obtained for the (0 1 1) orientation of the Ni_3Si alloy, giving a relative difference of 1.4 % respect to the (0 1 1) orientation value. This analysis of the interatomic distances and a/b ratio corroborates with the favorable formation of an alloyed layer of composition 3:1.

Going further in the increase of the coverage of Ni, on the structure of Fig. 6-a-snapshot IV, the adsorption of a new Ni atom is performed at four different sites on the surface, for a total of eleven Ni atoms. The same trend favoring mixing of Ni and Si species is observed. The initial and final positions are given in Appendix C. We observe that the Ni

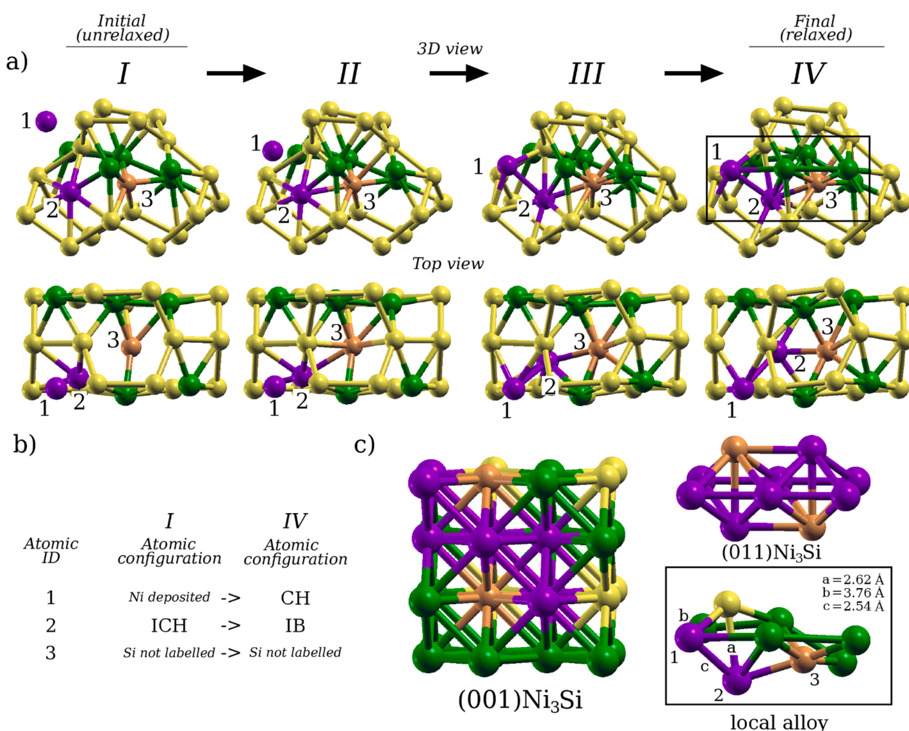

Fig. 6. Formation of a Ni:Si alloyed layer with 3:1 composition. a) Adsorption of the tenth Ni atom. The starting configuration contains nine Ni atoms already adsorbed: three in IDB and six in ICH (not all shown for readability – see Appendix C). The tenth deposition site is indicated by the position 1 in snapshot I. Snapshot IV shows the relaxed configuration after the tenth adsorption. The purple atom labelled 1 is the adsorbed nickel atom. The purple Nickel atom labelled 2 and the orange silicon atom labelled 3 are the displaced atoms changing local configurations upon adsorption. The frame in snapshot IV referred to frame in c). b) Adopted configurations of atoms 1, 2, 3 highlighted in a) from snapshots I and IV in a). c) Local silicide formed: unit cell of Ni_3Si is provided where the local alloy is highlighted using orange and purple colors. The correspondence with the local alloy is highlighted on the right with the help of the analysis on the distances altogether with an atomic positioning. Green and purple spheres are nickel atoms and yellow and orange spheres are silicon atoms. Purple and orange are used to highlight atom movements. (For interpretation of the references to colour in this figure legend, the reader is referred to the web version of this article.)

(position 1 in Appendix C) can still adsorb between the first and second layers, thus creating space between the pure silicon layers formed by the dimers. The corresponding adsorption energy is −4.84 eV. The Ni atom cannot be further inserted spontaneously in this specific configuration because the CH site below is already occupied. The final configuration presents an interesting mechanism, allowing the upper Si layer to penetrate more Ni on the surface by an upward movement of Si atoms, which could be favorable by the further mixing of Ni and Si species. On other the tested position (position 2 in Appendix C), typical configuration of a subsequent insertion in the substrate can be observed that is of interest for the understanding of the further mixing of the alloyed silicide layer. In particular, we observe that the deposited Ni atom takes place in a CH configuration, also pushing the ICH atom below towards the IB site, as observed above. The associated adsorption energy for this configuration is −4.29 eV, having a difference of 0.29 eV respect to the CH adsorption on pure Si surface. For other tested positions (for instance position 3 and 4 in Appendix C), no tendency of insertion is obtained, whereas interestingly the deposited Ni atoms seems to be attracted toward the adjacent dimer row, confirming the tendency of Ni to interact with the whole silicon surface. The adsorption energies for these configurations are −4.16 and −4.54 eV, respectively. We suppose here that these reached positions are brought to stabilize further according to the degree of alloying formed on the second dimer row of our surface. We do not study further the atomic diffusion from these adsorbed configurations for clear computational limitations and we concentrate on the high coverage on a given dimer row.

Returning more specifically to the adsorption from the tested position 2, we observe that this spontaneous adsorption is associated to the movement of several atoms, which finally validates that during this additional insertion the Ni atom inserts itself into the Si surface. A chemical environment similar in composition and interatomic distances with its first close neighbors characteristic of a Ni:Si layer of composition 3:1 is obtained, without activation barrier neither for diffusion nor for atomic reorganization at the interface.

4. Experimental investigations: X-ray reflectivity combined with High-Resolution Transmission Electron Microscopy

A special focus was addressed to a detailed characterization of the as deposited material and its interface with silicon by X-ray Reflectivity (XRR) analyses combined with High-Resolution Scanning Transmission Electron Microscopy analyses (HR-STEM). XRR is an analytical technique sensitive to the electronic density of the materials and indeed well suited to finely describe eventual Ni-Si intermixing and phase formation. Details of the sample preparations are given in Appendix D.

Fig. 7 shows the XRR profile of the as deposited sample with typical interference fringes that are related to the layer thickness. The critical angle measured on that profile corresponds to a density of 8.9 g/cm^3, the value expected for the pure Ni layer. A nickel layer is indeed found in the topmost part of the sample with thickness close to 8 nm. This value underestimates the deposited thickness. Accordingly, a description of a pure nickel layer on top of a silicon substrate is not exhaustive to properly fit the experimental curve. A refined model of the sample, which nicely fits the experimental data, includes a second layer in touch with the silicon substrate, as described in the inset of the figure. It consists of a 3 nm-thick Ni-Si mixed layer with density 8 g/cm^3, which corresponds to a Ni:Si ratio of 3:1.

A similar scenario was depicted by HR-STEM analyses as shown in the cross section of the as deposited sample of Fig. 8. The sample was prepared following a cold procedure described in appendix D, to avoid any sample modification. The topmost layer of nickel is made of nanometers grains that are mostly [1 1 1] oriented. A mixed layer is found immediately under the pure nickel layer as introduced by XRR. As an additional information, this layer has a low degree of lattice order (similar to an amorphous).

Ni-Si mixing with similar features was previously found in samples

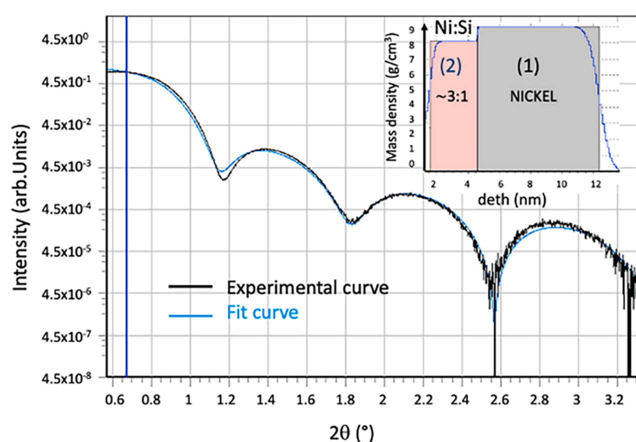

Fig. 7. XRR profile of the as deposited sample. A schematic of the layered structure and obtained composition is provided in the inset. red area reveals a Ni:Si with a composition of 3:1. The blue curve represents the fit arising from the model which is in good agreement with the experimental data. (For interpretation of the references to colour in this figure legend, the reader is referred to the web version of this article.)

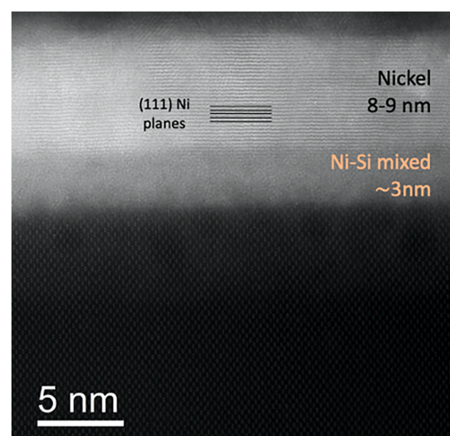

Fig. 8. HR-STEM cross-section of the as deposited sample. An amorphous Ni-Si mixed layer of 3 nm is clearly visible in between the brighter unreacted nickel layer on top and the dark silicon substrate at the bottom.

wherein the nickel layer was deposited by sputtering [16]. Since in evaporated layers the adatoms are expected to carry out less energy than sputtered counterparts, it is argued that intermixing occurs due to adsorption-diffusion-injection mechanisms as described in the theoretical dissertation independently of the deposition method. In addition, the observed Ni-Si mixing in a ratio 3:1 found by both experimental techniques corroborates a driving force for nickel insertion into the silicon lattice with a description provided by the experimental calculations.

5. Conclusion

In conclusion, the combination of first-principles calculations, XRR and HR-TEM experiments unambiguously shows the reactive interface formation during deposition where Ni adsorbs and inserts readily onto the clean surfaces of Si(0 0 1). This study provides an accurate description of the formation of a native surface alloyed layer during the deposition of Ni on the surface of the Si(0 0 1) substrate. This conclusion confirms the rapid formation of a Ni_3Si composition alloyed layer at the interface between Ni and Si.

We demonstrate that the formation of this alloyed layer occurs thermodynamically without activation barrier once the Ni coverage on

the surface is sufficient. The as-deposited interface formed before the activation of the silicidation process is then Si/Ni_3Si/Ni. However, for the simulation of the silicidation process with more realistic systems, it becomes more difficult to maintain *ab initio* accuracy, as they require long time and size scale simulations that cannot be obtained with *ab initio* calculations. For this, recourse to higher scale modelling, in particular Molecular Dynamics and Kinetic Monte Carlo, is necessary. For the former, there is a lack of accurate empirical potential and we are working on the development of an interatomic potential based on machine learning methods. For the latter, we are currently addressing the challenge of reproducing phase change and further studying the atomic dynamics at the interface between nickel silicides and silicon substrate, both regarding Ni and Si species.

6. Author credit statement

C.J. performed the DFT calculations and C.J. and A.H. performed related analysis. A.H., C.J., A.J., and J.L. analyzed the results and wrote the paper. Conceptualization by A.H.. A.A., C.B., A.LM, J.M. and G.L. wrote the experimental results.

A.H., C.J., A.A., and J.M. revised the manuscript.

All authors discussed and commented on the results and on the paper and its revision.

Declaration of Competing Interest

The authors declare that they have no known competing financial interests or personal relationships that could have appeared to influence the work reported in this paper.

Data availability

Data will be made available on request.

Acknowledgements

This work was performed using HPC resources from GENCI-A0090911942 and CALMIP- Grant P1418. The research leading to these results has received funding from the European Union's Horizon 2020 research and innovation program under grant agreement No. 871813 MUNDFAB. This work was partly supported by LAAS-CNRS micro and nanotechnologies platform member of the French RENATECH network.

Appendix A:. Stable sites on the Si(0 0 1) surface

We provide the six stable atomic structures of one adsorbed Ni atom on the Si(1 0 0) surface and their adsorption energies.

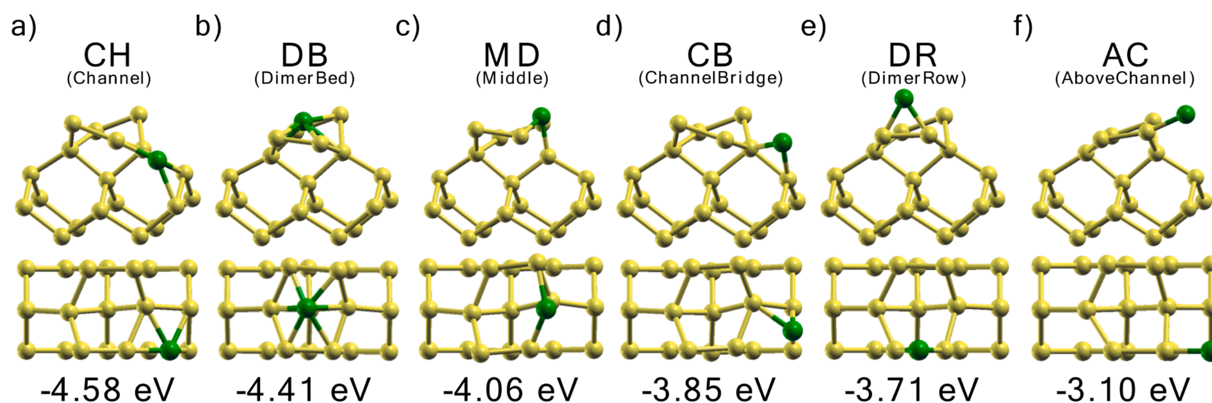

Appendix B:. Without concerted insertion, Ni does not diffuse deeply into the Si

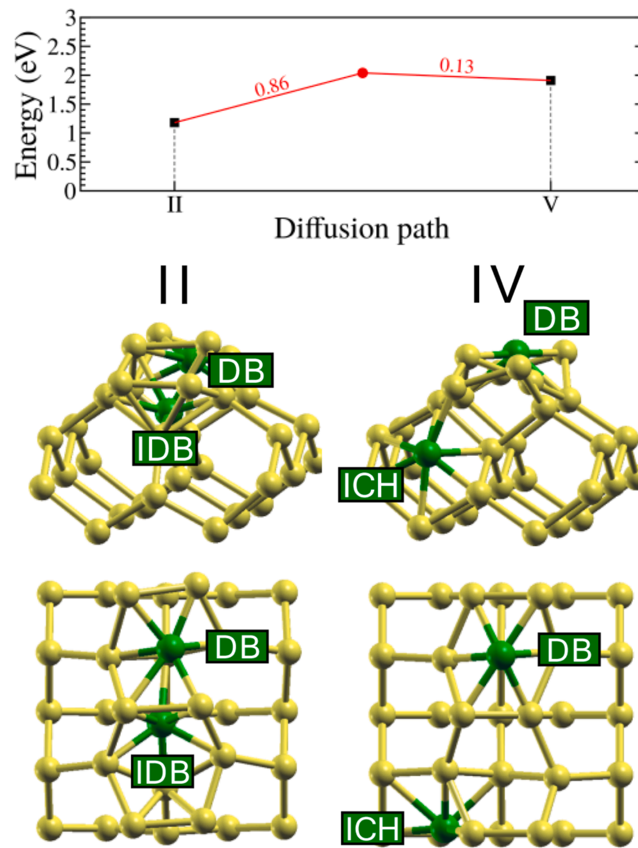

Appendix C:. Additional Ni deposition on a surface Ni_xSi_y alloyed pattern containing 10 inserted Ni atoms

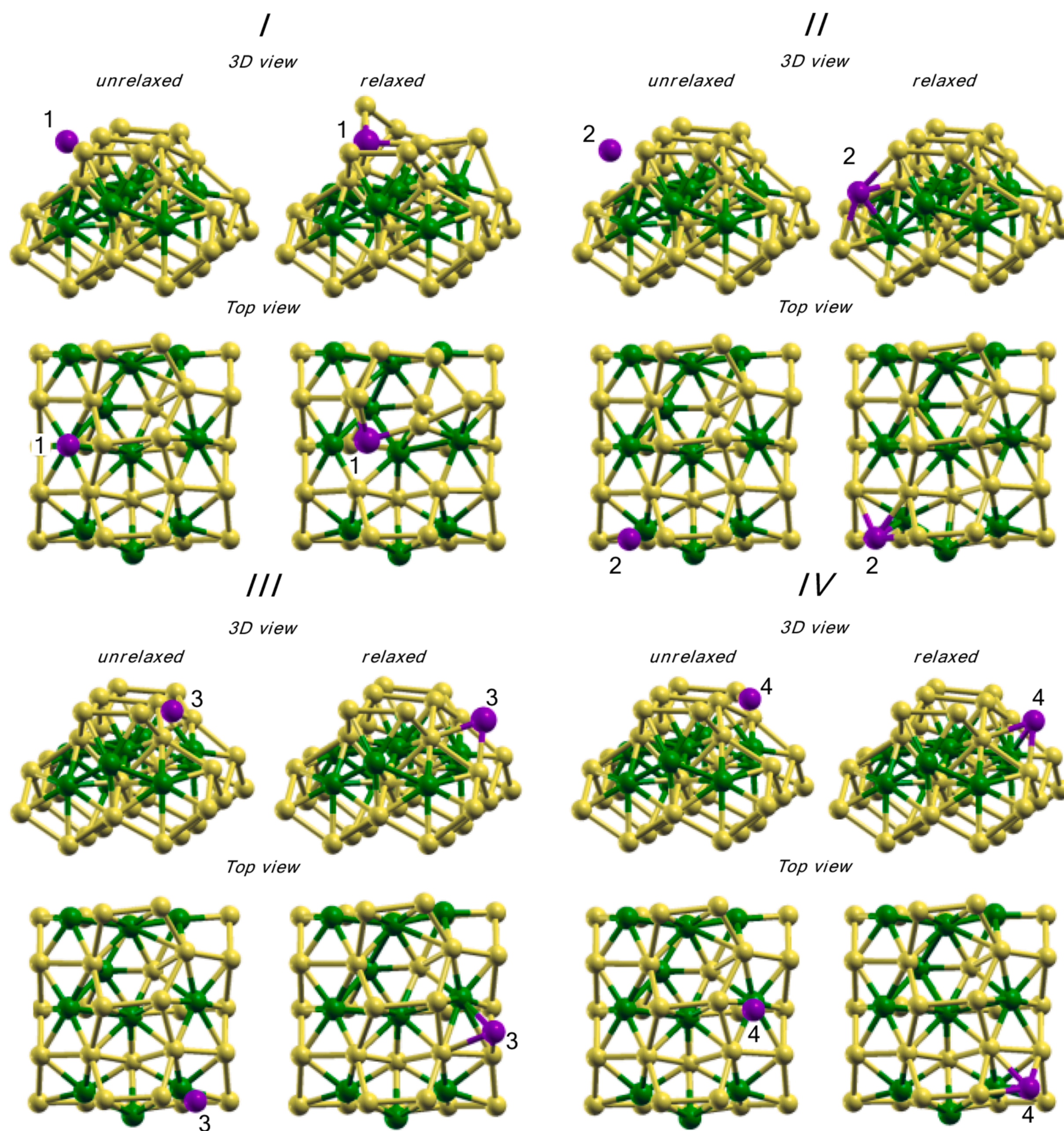

Appendix D:. Experimental details

Nickel silicide samples have been fabricated by physical vapor deposition (PVD) of nickel thin films on 4-inch wafers of lightly doped p-Si (1 0 0) (boron at 1×10^{15} at/cm^3). The wafers are firstly cleaned in piranha solution (H_2SO_4:H_2O_2 1:1) removing any organic residues on the surface. Then the native silicon oxide layer of 1–2 nm thickness is removed by wet chemical etching in diluted hydrofluoric acid. The cleaned wafer is immediately transferred into the vacuum chamber of a "Plassys MEB-550SL" electron-beam evaporator. To ensure an oxygen free surface, any native oxide having reformed during the transfer is removed by in-situ Ar milling prior to the PVD metallization. The Ar plasma is obtained at a 5 sccm flow of Ar with a chamber pressure of 6.5×10^{-5} mbar for 2 min. The 10 nm thick Nickel layer is deposited by thermal evaporation under ambient temperature conditions, without any additional heating, and at a low deposition rate of 0.1 nm/s with a beam power loading of 280 mA and 10 kV. The metallized wafers, upon retrieval, are kept under N_2 to avoid oxidization of the metallic surface before further processing or characterization.

For XRR analyses we used a D8-Discover Bruker AXS diffractometer with a Cu-ka source, a Goebel mirror, a 0.1 mm slit at the primary beam, a 0.2 mm slit, and a scintillator as a detector. The samples were used without any preparation procedure.

TEM sample preparation was carried out following a fully cold procedure. The samples were glued together at room temperature for two days, the preparation steps were carried out using cold glue and solvent removing bath, ion milling final step was performed under liquid nitrogen. Scanning Transmission Electron Microscopy analyses have been carried out in High Angle Annular Dark Field (HAADF) configuration using a Jeol Arm200 Microscope.

References

[1] N. Breil, C. Lavoie, B.F. Ozcan, N. Klymko, K. Nummy, B. Sun, S.J. Jordan, J. Yu, F. Zhu, S. Narasimha, M. Chudzik, Challenges of nickel silicidication in CMOS technologies, Microelectron. Eng. 137 (2015) 79–87, https://doi.org/10.1016/j.mee.2014.12.013.

[2] A. Lauwers, A. Steegen, M. de Potter, R. Lindsay, A. Satta, H. Bender, K. Maex, Materials aspects, electrical performance, and scalability of Ni silicide towards sub-0.13 μm technologies, Journal of Vacuum Science & Technology B: Microelectronics and Nanometer Structures Processing, Measurement, and Phenomena 19 (2001) 2026–2037, https://doi.org/10.1116/1.1409389.

[3] J. Kittl, Q. Hong, H. Yang, N. Yu, S. Samavedam, M. Gribelyuk, Advanced salicides for 0.10 μm CMOS: Co salicide processes with low diode leakage and Ti salicide processes with direct formation of low resistivity C54 TiSi2, Thin Solid Films 332 (1998) 404–411, https://doi.org/10.1016/S0040-6090(98)01017-7.

[4] S.-L. Zhang, M. Ostling, Metal silicides in CMOS technology: Past, present, and future trends, Crit. Rev. Solid State Mater. Sci. 28 (2003) 1–129, https://doi.org/10.1080/10408430390802431.

[5] A. Reader, A. Van Ommen, P. Weijs, R. Wolters, D. Oostra, Transition metal silicides in silicon technology, Rep. Prog. Phys. 56 (1993) 1397, https://doi.org/10.1088/0034-4885/56/11/002.

[6] M. Hannula, K. Lahtonen, H. Ali-Löytty, A. Zakharov, T. Isotalo, J. Saari, M. Valden, Fabrication of topographically microstructured titanium silicide interface for advanced photonic applications, Scr. Mater. 119 (2016) 76–81, https://doi.org/10.1016/j.scriptamat.2016.03.016.

[7] B.-Y. Tsaur, C. Chen, J.-P. Mattia, PtSi Schottky-barrier focal plane arrays for multispectral imaging in ultraviolet, visible, and infrared spectral bands, IEEE Electron Device Lett. 11 (1990) 162–164, https://doi.org/10.1109/55.61783.

[8] K. Kim, Y. Kang, S. Yun, C. Yang, E. Jung, J. Hong, K. Kim, Reduced On-Resistance and Improved 4H-SiC Junction Barrier Schottky Diodes Performance by Laser Annealing on C-Face Ohmic Regions in Thin Structures, Coatings 12 (2022) 777, https://doi.org/10.3390/coatings12060777.

[9] B. Sarpi, R. Zirmi, M. Putero, M. Bouslama, A. Hemeryck, S. Vizzini, Growth stability and decomposition of Mg2Si ultra-thin films on Si(100), Appl. Surf. Sci. 427 (2018) 522, https://doi.org/10.1016/j.apsusc.2017.09.027.

[10] B. Sarpi, N. Rochdi, R. Daineche, M. Bertoglio, C. Girardeaux, A. Baronnet, J. Perrin- Toinin, M. Bocquet, M. Djafari-Rouhani, A. Hemeryck, S. Vizzini, Oxidation of Mg atomic monolayer onto silicon: A road toward MgOx/Mg2Si (11–1)/Si (100) heterostructure, Surf. Sci. 642 (2015) L1, https://doi.org/10.1016/j.susc.2015.08.003.

[11] A. Lauwers, M. De Potter, O. Chamirian, R. Lindsay, C. Demeurisse, C. Vrancken, K. Maex, Silicides for the 100-nm node and beyond: Co-silicide, Co (Ni)-silicide and Ni-silicide, Microelectron. Eng. 64 (2002) 131–142, https://doi.org/10.1016/S0167-9317(02)00777-3.

[12] H. Brahmi, S. Ravipati, M. Yarali, S. Shervin, W. Wang, J.-H. Ryou, A. Mavrokefalos, Electrical and optical properties of sub-10 nm nickel silicide films for silicon solar cells, J. Phys. D Appl. Phys. 50 (2016), https://doi.org/10.1088/1361-6463/50/3/035102.

[13] C. Lavoie, P. Adusumilli, A.V. Carr, J.S. Sweet, A.S. Ozcan, E. Levrau, N. Breil, E. Alptekin, Contacts in Advanced CMOS: History and Emerging Challenges, ECS Trans. 77 (2017) 59, https://doi.org/10.1149/07705.0059ecst.

[14] G. Larrieu, Y. Guerfi, X.L. Han, N. Clément, Sub-15 nm gate-all-around field effect transistors on vertical silicon nanowires, Solid State Electron. 130 (2017) 9–14, https://doi.org/10.1016/j.sse.2016.12.008.

[15] K. De Keyser, C. Van Bockstael, R. Van Meirhaeghe, C. Detavernier, E. Verleysen, H. Bender, W. Vandervorst, J. Jordan-Sweet, C. Lavoie, Phase formation and thermal stability of ultrathin nickel-silicides on Si (100), Appl. Phys. Lett. 96 (2010), 173503, https://doi.org/10.1063/1.3384997.

[16] F. Geenen, E. Solano, J. Jordan-Sweet, C. Lavoie, C. Mocuta, C. Detavernier, The influence of alloying on the phase formation sequence of ultra-thin nickel silicide films and on the inheritance of texture, J. Appl. Phys. 123 (2018), 185302, https://doi.org/10.1063/1.5022070.

[17] A. Alberti, A. La Magna, Role of the early stages of Ni-Si interaction on the structural properties of the reaction products, Journal of Applied Physics 114 11 1 (2013), https://doi.org/10.1063/1.4818630.

[18] H. Iwai, T. Ohguro, S.-I. Ohmi, NiSi salicide technology for scaled CMOS, Microelectron. Eng. 60 (2002) 157–169, https://doi.org/10.1016/S0167-9317(01)00684-0.

[19] M.B. Khan, D. Deb, J. Kerbusch, F. Fuchs, M. Löffler, S. Banerjee, U. Mühle, W. M. Weber, S. Gemming, J. Schuster, A. Erbe, Y.M. Georgiev, Towards Reconfigurable Electronics: Silicidation of Top-Down Fabricated Silicon Nanowires, Appl. Sci. 9 (2019) 3462, https://doi.org/10.3390/app9173462.

[20] J. Gao, A. Malchère, S. Yang, A. Campos, T. Luo, K. Quertite, P. Steyer, C. Girardeaux, L. Zhang, D. Mangelinck, Dewetting of Ni silicide thin film on Si substrate: In-situ experimental study and phase-field modeling, Acta Mater. 223 (2022), https://doi.org/10.1016/j.actamat.2021.117491.

[21] M. Grégoire, F. Morris Anak, S. Verdier, K. Dabertrand, S. Guillemin, D. Mangelinck, On the influence of Ni(*Pt*)Si thin film formation on agglomeration threshold temperature and its impact on 3D imaging technology integration, Microelectron. Eng. 271–272 (2023), 111937, https://doi.org/10.1016/j.mee.2023.111937.

[22] A. Alberti, C. Bongiorno, B. Cafra, G. Mannino, E. Rimini, T. Metzger, C. Mocuta, T. Kammler, T. Feudel, Pseudoepitaxial transrotational structures in 14 nm-thick NiSi layers on [001] silicon, Acta Crystallographica B 61 (2005) 486, https://doi.org/10.1107/S0108768105022585.

[23] A. Alberti, C. Bongiorno, P. Alippi, A. La Magna, C. Spinella, E. Rimini, Structural characterization of Ni2Si pseudoepitaxial transrotational structures on [001] Si, Acta Crystallographica B 62 (2006) 729, https://doi.org/10.1107/S0108768106029727.

[24] A. Alberti, C. Bongiorno, E. Rimini, M.G. Grimaldi, Critical nickel thickness to form silicide transrotational structures on [001] silicon, Appl. Phys. Lett. 89 (10) (2006), https://doi.org/10.1063/1.2338019.

[25] A. Schrauwen, K. Van Stiphout, J. Demeulemeester, B. De Schutter, W. Devulder, C. M. Comrie, C. Detavernier, K. Temst, A. Vantomme, The role of composition and microstructure in Ni–W silicide formation and low temperature epitaxial NiSi2 growth by premixing Si, J. Phys. D Appl. Phys. 50 (2017), 065303, https://doi.org/10.1088/1361-6463/aa4ed7.

[26] M. Christensen, V. Eyert, C. Freeman, E. Wimmer, A. Jain, J. Blatchford, D. Riley, J. Shaw, Formation of nickel-platinum silicides on a silicon substrate: Structure, phase stability, and diffusion from ab initio computations, J. Appl. Phys. 114 (2013), 033533, https://doi.org/10.1063/1.4816094.

[27] T. Hiramatsu, T. Takashi, M.Y. Yang, K. Kamiya, K. Shiraishi, T. Nakayama, First-principles evaluation of penetration energy of metal atom into Si substrate, Jpn. J. Appl. Phys. 53 (2014), 058006.

[28] R.K. Pandey, G. Maity, S. Pathak, P. Kalita, S. Dubey, New insights on Ni-Si system for microelectronics applications, Microelectron. Eng. 264 (2022), 111871, https://doi.org/10.1016/j.mee.2022.111871.

[29] A.-Y. Hou, Y.-H. Ting, K.-L. Tai, C.Y. Huang, K.-C. Lu, W.-W. Wu, Appl. Surf. Sci. 538 (2021), 148129, https://doi.org/10.1016/j.apsusc.2020.148129.

[30] T.T. Tran, C. Lavoie, Z. Zhang, D. Primetzhofer, In-situ nanoscale characterization of composition and structure during formation of ultrathin nickel silicide, Appl. Surf. Sci. 536 (2021), 147781, https://doi.org/10.1016/j.apsusc.2020.147781.

[31] S. Bhan, H. Kudielka, Ordered bcc-phases at high temperatures in alloys of transition metals and B-subgroup elements, Int. J. Mater. Res. 69 (1978) 333–336, https://doi.org/10.1515/ijmr-1978-690510.

[32] J. Fouet, M. Texier, M.-I. Richard, A. Portavoce, D. Mangelinck, C. Guichet, N. Boudet, O. Thomas, Silicide formation during reaction between Ni ultra-thin films and Si (001) substrates, Mater. Lett. 116 (2014) 139–142, https://doi.org/10.1016/j.matlet.2013.10.119.

[33] E.J. Van Loenen, J.F. Van Der Veen, F.K. LeGoues, Ni-Si mixing: A new model for low temperature silicide formation, Surf. Sci. 157 (1985) 1–16, https://doi.org/10.1016/0039-6028(85)90631-4.

[34] Y.-J. Chang, J.L. Erskine, First phase nickel silicide nucleation and interface structure at Si(100) surfaces, J. Vac. Sci. Technol. A 1 (1983) 1193–1197, https://doi.org/10.1116/1.571896.

[35] R. Kilper, S. Teichert, P. Oelhafen, In situ investigation of the formation of an intermixed phase at the Ni/Si(100) interface by photoelectron spectroscopic methods, Appl. Surf. Sci. 123–124 (1998) 550–554, https://doi.org/10.1016/S0169-4332(97)00569-2.

[36] D. Sarkar, M. Falke, H. Giesler, S. Teichert, G. Beddies, H.-J. Hinneberg, Role of buried ultra thin interlayer silicide on the growth of Ni film on Si(100) substrate, Appl. Phys. A 70 (2000) 681–684, https://doi.org/10.1007/s003390050015.

[37] L. Ehouarne, M. Putero, D. Mangelinck, F. Nemouchi, T. Bigault, E. Ziegler, R. Coppard, In situ study of the growth kinetics and interfacial roughness during the first stages of nickel–silicide formation, Microelectron. Eng. 83 (2006) 2253–2257, https://doi.org/10.1016/j.mee.2006.10.014.

[38] P. Hohenberg, W. Kohn, Inhomogeneous electron gas, Phys. Rev. 136 (1964) B864, https://doi.org/10.1103/PhysRev.136.B864.

[39] W. Kohn, J.L. Sham, Self-Consistent Equations Including Exchange and Correlation Effects, Phys. Rev. 140 (1965) A1133, https://doi.org/10.1103/PhysRev.140.A1133.

[40] P. Giannozzi, et al., QUANTUM ESPRESSO: a modular and open-source software project for quantum simulations of materials, J. Phys. Condens. Matter 21 (2009), 395502, https://doi.org/10.1088/0953-8984/21/39/395502.

[41] P. Giannozzi, et al., Advanced capabilities for materials modelling with Quantum ESPRESSO, J. Phys. Condens. Matter 29 (2017), 465901, https://doi.org/10.1088/1361-648X/aa8f79.

[42] J.P. Perdew, K. Burke, M. Ernzerhof, Generalized Gradient Approximation Made Simple, Physical Review Letter 77 (1996) 3865, https://doi.org/10.1103/PhysRevLett.77.3865.

[43] P.E. Blöchl, Projector augmented-wave method, Phys. Rev. B 50 (1994) 17953, https://doi.org/10.1103/PhysRevB.50.17953.

[44] N. Mousseau, L.K. Béland, P. Brommer, J.F. Joly, F. El-Mellouhi, E. Machado-Charry, M.C. Marinica, P. Pochet, The Activation-Relaxation Technique: ART Nouveau and Kinetic ART, J. Phys. B Atomic Mol. Phys. 2012 (2012), 925278, https://doi.org/10.1155/2012/925278.

[45] A. Jay, C. Huet, N. Salles, M. Gunde, L. Martin-Samos, N. Richard, G. Landa, V. Goiffon, S. De Gironcoli, A. Hémeryck, N. Mousseau, Finding Reaction Pathways and Transition States: r-ARTn and d-ARTn as an Efficient and Versatile Alternative to String Approaches, J. Chem. Theory Comput. 16 (2020) 6726–6734, https://doi.org/10.1021/acs.jctc.0c00541.

[46] A. Jay, M. Gunde, N. Salles, M. Poberznik, L. Martin-Samos, N. Richard, S. de Gironcoli, N. Mousseau, A. Hémeryck, Activation-Relaxation Technique: an efficient way to find minima and saddle points of potential energy surfaces, Computational Materials Sciences 209 (2022), 111363, https://doi.org/10.1016/j.commatsci.2022.111363.

[47] M. Poberznik, M. Gunde, N. Salles, A. Jay, A. Hémeryck, N. Richard, N. Mousseau, L. Martin-Samos, ARTn gets plugin-ized: implementation of the Activation Relaxation Technique as a biased minimization – to be published.
[48] A. Ramstad, G. Brocks, P. Kelly, Theoretical study of the Si (100) surface reconstruction, Phys. Rev. B 51 (1995) 14504, https://doi.org/10.1103/PhysRevB.51.14504.
[49] A. Hemeryck, N. Richard, A. Estève, M. Djafari Rouhani, Multi-scale modeling of oxygen molecule adsorption on a Si(100)-p(2×2) surface, J. Non Cryst. Solids 353 (2007) 594–598, https://doi.org/10.1016/j.jnoncrysol.2006.10.030.